Chapter 4
Tungsten-based broadband perfect metamaterial absorber from visible to near-infrared regions

Utilizing solar radiations mainly concentrated in the optical region requires the perfect absorption of light by photovoltaic cells. In this chapter, we have demonstrated a broadband-perfect metamaterial absorber (PMA) based on tungsten (W) metal in the visible to near-infrared region. The proposed metamaterial absorber has a 98% average absorbance for the 375-1100 nm wavelength region. A very large absorption bandwidth of over 90% is obtained, and the maximum absorption is around the unity. The polarization-insensitive-based proposed absorber tolerates a large incident for both transverse magnetic (TM) and transverse electric (TE) modes. Moreover, we have investigated the optimization of the geometric parameters of the unit cell to gain good absorption results. The proposed absorber shows a promising expectance in various applications such as solar energy harvesting, solar cell, thermal imaging, photodetectors, and durable optoelectronics devices.

4.1 Introduction

Methods for the design and study of metamaterial absorbers that exhibit broadband absorption in the visible regions were shown in previous chapters. To obtain more absorption, in this chapter, we have used a square ring-shaped resonator that shows broadband absorption in the visible to near-infrared regions. The mentioned absorber model metamaterials exhibit properties of double negative characteristics, polarization-independent, wide incident angles, absorption performances, conversion efficiency, and other important results that can be used for solar energy harvesting applications.

In recent years, Metamaterials (MTMs) have attracted considerable attraction due to their incredible performance to change and manipulate incident electromagnetic (EM) waves which motivated researchers to focus on metamaterial for different applications. The first metamaterial (MTM) absorber[72] was investigated by Landy et al. in 2008. MTM is an artificial material with a sub-wavelength metal-dielectric structure. The properties like effective permittivity $\varepsilon(\omega)$, permeability $\mu(\omega)$, and refractive index (n) of metamaterials have negative values[6]. Metamaterials are used across various frequency regions such as gigahertz, terahertz, and optical for many purposes such as antenna[112], filter[187], sensors[188], waveguides[189], and perfect absorber[116]. Metamaterials show perfect absorption in a particular range of frequency, which prefers some additional applications such as solar thermophotovoltaics[93], emitters[190], and photodetectors[124]. Metamaterial absorbers have generally consisted of two-layer[116], three-layer[191], four-layer[110], and multilayers[192], but most of the commonly used metamaterials have a three-layer[193] (metal-dielectric-metal) structure. The dielectric layer absorbs the incident light and generates the coupling capacitance between the resonator and metal layers. The plasmonic resonance of the GaAs plane and the symmetrical structure are also reasons for large

absorption. However, the impedance of metamaterial match with free space is the main reason for near-perfect absorption. These properties are utilized to obtain electrical energy by utilizing electromagnetic energy and used in thermo-photovoltaic devices such as absorber[123], emitter[194], photodetctors[124], etc. It is recently reported that solar radiation could be captured by the metamaterial and improve the efficiency of photovoltaic devices. Mostly the solar spectrum covered the visible region from 400 nm to 750 nm wavelengths. Therefore, we need high absorption for the solar cells and a suitable MTM provides the maximum absorption in this range, which can be utilized for energy harvesting applications. Recently, several metamaterial absorbers have been provided the single-band[128], dual-band[129], multi-band[130], and broadband[191] absorber to improve the energy harvesting in the solar cell.

The earth contains solar energy in different radiation forms, which are visible (48%), infrared (43%), and ultraviolet (7.5%). The visible and infrared radiations are mostly used for potential applications such as solar cells which provide the maximum current at the output. The high transmission and large reflections reduce the conversion efficiency of a solar cell. Most of the reported absorbers covered only some portion of visible light and show the minimum conversion efficiency is not suitable for that application[143]. Moreover, the short circuit current density (J_{sc}) is another characteristic of global performance that plays a crucial role in solar cell characteristics[146]. Recently reported research papers, J_{sc} has been investigated with different thicknesses of the dielectric layer that shows the J_{sc} in visible to near-infrared range under the AM1.5 solar illuminations[27]. We require the large J_{sc} and high solar energy trapping on the absorber which should be near-unity due to multiple coupling of resonances for potential applications. Our purpose is to improve the conversion efficiency and short-circuit current density for photovoltaic applications.

In this chapter, we proposed a perfect broadband absorber composed of the dielectric material of gallium arsenide (GaAs) and tungsten (W) metal (refractory). The structural absorber consists of three layers, in which the top and bottom layers are made of W metal, and the ultrathin intermediate layer is made of GaAs. The range of 375-1100 nm exhibits a broadband absorbance with a large bandwidth (725 nm) and achieved an average absorbance of over 98%. The reason for selecting the tungsten metal is because it has a high melting point (3422 °C), withstands high temperatures, and matched the impedance with free space. The proposed geometrical structure is generated by the plasmonic resonance characteristics for the whole spectrum. The absorption characteristics also investigated different geometric and material parameters of the structures. Near unity, the real part of the impedance is the main reason to exhibit higher design structure absorption. Moreover, we have also investigated the effect of incident angles for TE and TM modes on the proposed structure's absorption. The proposed absorber is capable to improve conversion efficiency under the solar spectrum of solar cells and demonstrated the large value of conversion efficiency ($A_{AM1.5}$). It can be widely used for thin-film solar cells, solar energy harvesting, and thermal emitters.

4.2 Design and Simulation

4.2.1 Geometry and Materials

Fig. 4.1(a) shows the proposed perfect metamaterial absorber (PMA) consisting of three basic layers: (i) a bottom metallic layer with the thickness (h_1), (ii) a dielectric spacer with the thickness (h_2), and (iii) metallic resonators with the thickness (t). The value of all parameters is shown in Table 4.1. The structure has two parts of metal layers whereas the dielectric layer is made up of Gallium Arsenide (GaAs), and both metal layers are made up of Tungsten (W). The GaAs is chosen because it has some vital advantages, such as high efficiency, high electron

velocity and mobility, low-temperature coefficient, low light performance, flexibility, etc. GaAs have a direct bandgap that forms a good solar energy absorber. The GaAs also provide a good melting point in which property is desired for the dielectric layer as well[28]. The description of GaAs are $\varepsilon = 12.94$, $\tan\delta$ = 0.006, ρ = 5320 [kg/m^3] and the thermal conductivity (K) = 54 [W/K/m]. To obtain better efficiency in the solar thermo-photovoltaics (STPVs) require the higher temperature capability of the absorber. It is possible by the bottom layer of the absorber because tungsten metal has a high melting point (3422 °C) which provides high thermal stability with the absorber. When the light beam hits on the hot layer then it absorbs a large quantity of energy with the help of temperature difference. The melting point of the tungsten will withstand the higher energy. The increased stability of the absorber can be used in terrestrial applications. In the simulation process, the optical properties of tungsten metal (optical Palik) were taken from reference[140]. The main reason for choosing tungsten metal for the resonator and ground layer is because it is capable to match the high impedance with free space. This metal can improve the absorption spectra and decrease the transmission and reflection near zero because it has high intrinsic losses.

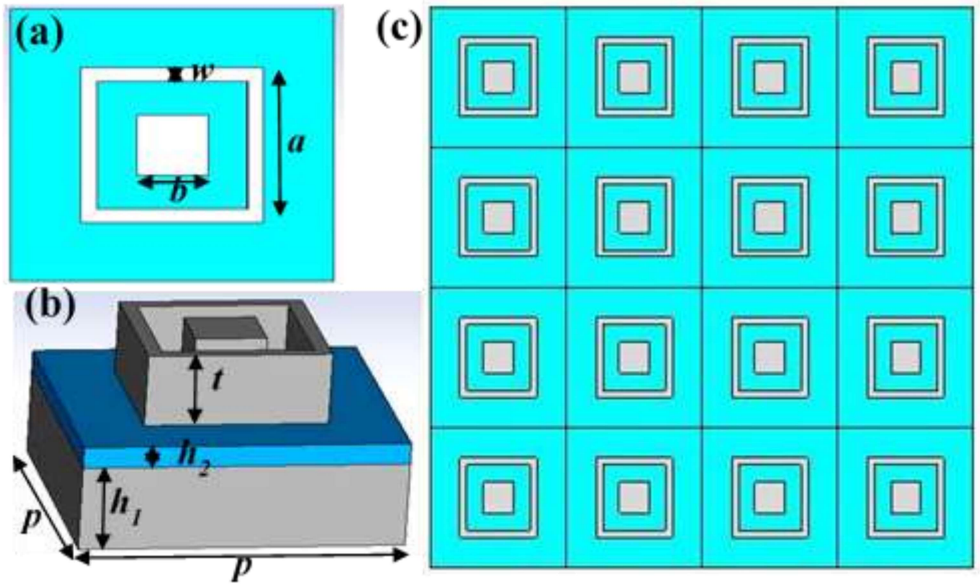

Fig. 4.1 (a) A front view of the absorber, **(b)** a schematic design of the proposed absorber, **(c)** structure of the unit cell in periodic series.

Table 4.1 Respective Values (nm) of the proposed absorber.

Parameter	***p***	***h*$_1$**	***h*$_2$**	***t***	***a***	***b***	***w***
Value (nm)	610	200	28	170	344	134	60

4.2.2 Methodology and absorption of the proposed unit cell

In the present work, the arrangement of the square ring-shaped resonator at the top of a dielectric spacer plays a crucial role in the optimization of the MTM absorber, which suggests that matched the impedance of metamaterial with free space impedance, i.e., $Z(\omega) = Z_0$.Eq. 4.1 helps to calculate the absorption of the metamaterial absorber[128].

$$A(\omega) = 1 - R(\omega) - T(\omega) \qquad (4.1)$$

Where, R (ω) and T(ω) represent the reflectance and transmittance depends on the scattering parameters i.e., $R(\omega) = |S_{11}(\omega)|^2$ and $T(\omega) = |S_{21}(\omega)|^2$.In the designed metamaterial absorber, the bottom layer's thickness is considered more than the skin depth, so it works as a reflector in the applied region, and the transmitted waves cannot pass through the structure. Therefore, transmission T(ω) becomes approximately zero in the above equation 4.1. Therefore, Eq. 4.1 can be written as:

$$A(\omega) = 1 - R(\omega) = 1 - |S_{11}(\omega)|^2 \quad (4.2)$$

Fig. 4.2(a) demonstrated the transmittance and reflectance with absorption for the given dimensions with gallium arsenide and tungsten. The proposed metamaterial absorber is shown broadband absorption while the transmittance is nearly zero and the reflectance is minimum. The proposed absorber has a 98% average absorption from 375 to 1100 nm regions. We also achieved three maximum peaks in the applied region, which are 441.80 nm, 506.88 nm, and 744.01 nm, respectively giving the maximum absorption values of 99.79%, 99.70%, and 99.94%. From 422 to 962 nm wavelength, the absorber has a >99% average absorption. Fig. 4.2(b) demonstrated the impedance matching conditions, where the real part of the impedance is around the unity and the imaginary part is approximately zero and makes a perfect absorber. From the parametric retrieval method[30], the normalized impedance can be calculated using the S-parameters by Eq. 4.3. This is a conventional equation for obtaining the effective impedance[6] (real and imaginary).

$$Z_{eff} = \sqrt{\frac{(1+S_{11})^2 - S_{21}^2}{(1-S_{11})^2 - S_{21}^2}} \quad (4.3)$$

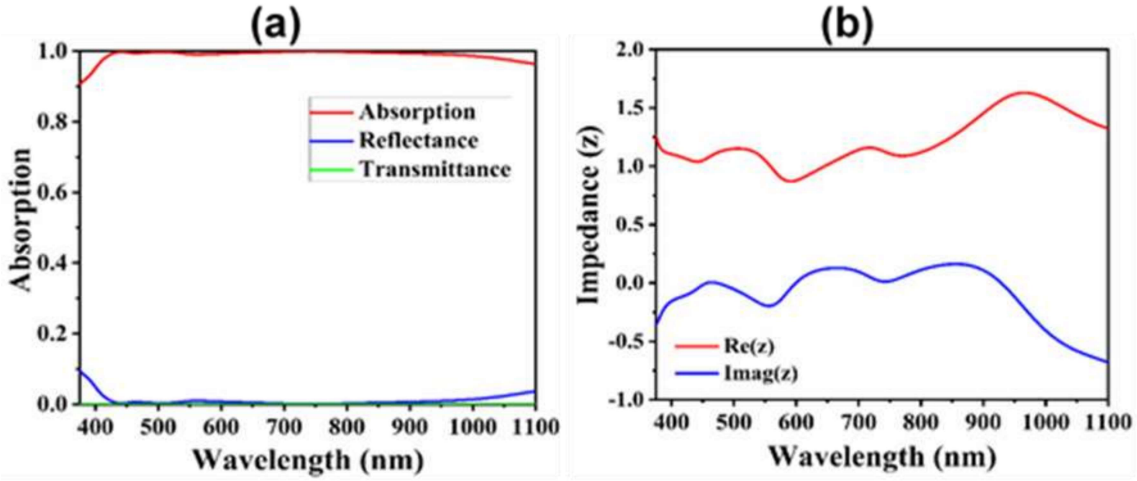

Fig. 4.2 (a) Absorption spectra of perfect metamaterial absorber, **(b)** effective impedance (real and imaginary) of the proposed absorber.

4.2.3 Simulation software and boundary conditions

S-parameters help to obtain the desired absorption level. It is essential to have convenient boundary conditions with the correct simulation setup. In this design, we have used the periodic boundary conditions in the x and y-direction, respectively. The propagation wave source is always passed through the z-direction and considers the perfectly matched layer (PML) with open spaces in the negative direction, which works as abolished scattering. In this method, the simulation software analyzer just repeats unit cell geometry in the same dimension and orientation to make a periodic array. The 2-D periodic structure array of the proposed absorber is illustrated in Fig. 4.1(c). The numerical analysis is carried out by CST software which is based on the finite integration technique (FIT) method to solve Maxwell's equations[122].

4.3 Results and discussion

4.3.1 Absorption characteristics

The design structure is separated into two layers to grasp the absorption characteristics. Metasurface (W) and the dielectric substrate (GaAs) made a front layer while the back layer consists only of the bottom layer of tungsten metal. The contribution of the absorption with the back layer and the front layer is represented in Fig. 4.3. The average absorption of the front layer is 72.88 % while the average absorption of the back layer is 50.68%. The tungsten's back layer has maximum absorption at the wavelength of 570.75 nm due to the intrinsic loss inside. The inductive and conductive properties of the resonators and lossless characteristics of the GaAs play a vital role in the absorption in the front layer. Therefore, the magnitude contributions of the absorption from both layers (back and front) is maximum, and it has shown the 98% average absorption which is the broadband absorption in this region and shown as the red curve in Fig. 4.3.

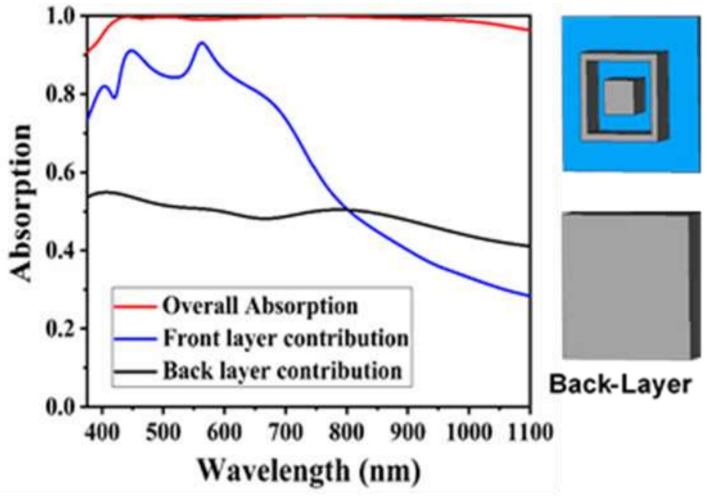

Fig. 4.3 Absorption spectra with back-layer of tungsten metal, and front-layer (dielectric and resonator).

4.3.2 Cross-polarization and Co-polarization with polarization conversation ratio

However, when designing and simulating the metamaterial (MTM) absorber, one question still arises: the MTM absorber must not work as a polarization converter. Always discuss the value of the polarization conversion ratio (PCR) instead of the absorption. The simulated symmetrical design method demonstrated the components of Cross-polarization and Co-polarization in Fig. 4.4(a) and 4.4(b) to diminish that question[122,142]. In the linear magnitude scale, the cross-polarization component is around zero, which confirms that the absorber did not convert the waves in the region.

$$|S_{11}(w)|^2 = |R_{yx}|^2 + |R_{yy}|^2 \quad (4.4)$$

$$|S_{11}(w)|^2 = |R_{xy}|^2 + |R_{xx}|^2 \quad (4.5)$$

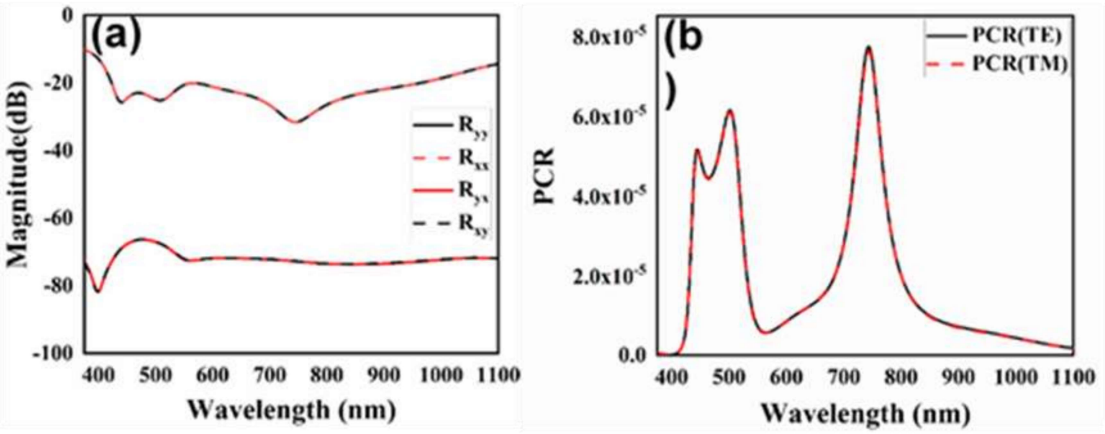

Fig. 4.4 (a) Cross-polarization and Co-polarization components in magnitude (dB), **(b)** PCR for TE and TM mode.

Here, R_{yy} and R_{xx} are the co-polarization components, R_{xy} and R_{yx} are the cross-polarization components. The value of PCR can be evaluated by Eqs. 4.6 and 4.7 using linear values of R_{yy}, R_{xx}, R_{yx}, and R_{xy} exhibited in Fig. 4.4(b). For both TE and TM modes, the PCR values are near zero.

$$PCR_{TE} = (R_{yx}^2)/ (R_{yx}^2 + R_{yy}^2) \quad (4.6)$$

$$PCR_{TM} = (R_{xy}^2)/ (R_{xy}^2 + R_{xx}^2) \quad (4.7)$$

4.3.3 Parametric analysis of the unit cell

To observe the absorption characteristics, it is necessary to know the effect of the absorber's geometric parameters. For the absorption mechanism, the parameters of the structure such as periodicity (p), dielectric thickness (h_2), resonator thickness (t), and resonator width (w) are very important and report the variation of absorption spectra. Firstly, we examined the absorber's periodicity effect represented by the parameter (p) in Fig. 4.5(a). When sweeps the unit cell period, then all resonance peaks are more affected by the original peaks. It generates by the resonators because E-field and H-field were changing their positions. Therefore, if changed the periodicity, maximum absorptions are affected and show absorption somewhere high and low. We chose the possible period (p = 610 nm) for the metamaterial absorber to achieve perfect absorption. We have also examined the thickness effect of the dielectric layer (GaAs) represented by the parameter (h_2). The dielectric layer thickness can modulate the resonance wavelength and absorption rate, as shown in Fig. 4.5(b). It mainly helps the coupling between the resonators and the ground layer. Therefore, the magnetic response is generated by this coupling. Thus, the impedance matching of the absorber with the free space verified the electric and magnetic distribution. So, the thickness of dielectric separation generates the magnetic response when the thickness is smaller and higher than 28 nm. This condition does not verify the impedance matching for some layer thicknesses. Therefore, the thickness is significant for considering the design of the absorber.

In the absorber design, the dimensions of resonator selection should be careful because it plays a crucial role in perfect absorption. The changes in the dimension of resonators affect the absorption spectrum while keeping constant to the other parameters. The results with different dimensions are shown in Fig. 4.5(c). The red color indicates the desired results for maximum absorption. The optimum thickness is 170 nm required for the perfect absorption checking with other thickness parameters. So the absorption peak shifts when its thickness increases and decreases, and we need an ideal thickness of resonators to generate the perfect absorption and create suitable magnetic and electric resonances. As seen in Fig. 4.5(d), the resonance wavelength is also dependent on the width of the resonators. So in this section, we have explained the width (*w*) of the square ring-shaped resonator. When sweeps the resonators' width, the absorption result varies with different wavelengths in the broadband region. However, the maximum peaks of the absorption at 441.80 nm, 506.88 nm, and 744.01 nm are strongly dependent on the resonators' width that gives the electric and magnetic responses for the different results. Therefore, to find the perfect absorption, it is necessary to adjustment of the width. Thus, the square ring-shaped resonator at the same wavelength gives different absorption results with the resonators' width. The best absorption results with width (w = 60 nm) at the described wavelength are shown in Fig. 4.5(d). Here is also shown the absorption with the various wavelength at the different thicknesses and widths of resonators. Therefore, the thickness of the dielectric layer and resonators, the dielectric layer's width, and the dimensions of resonators are very important to make a unit cell of metamaterial structure that gives the perfect absorption within wavelengths.

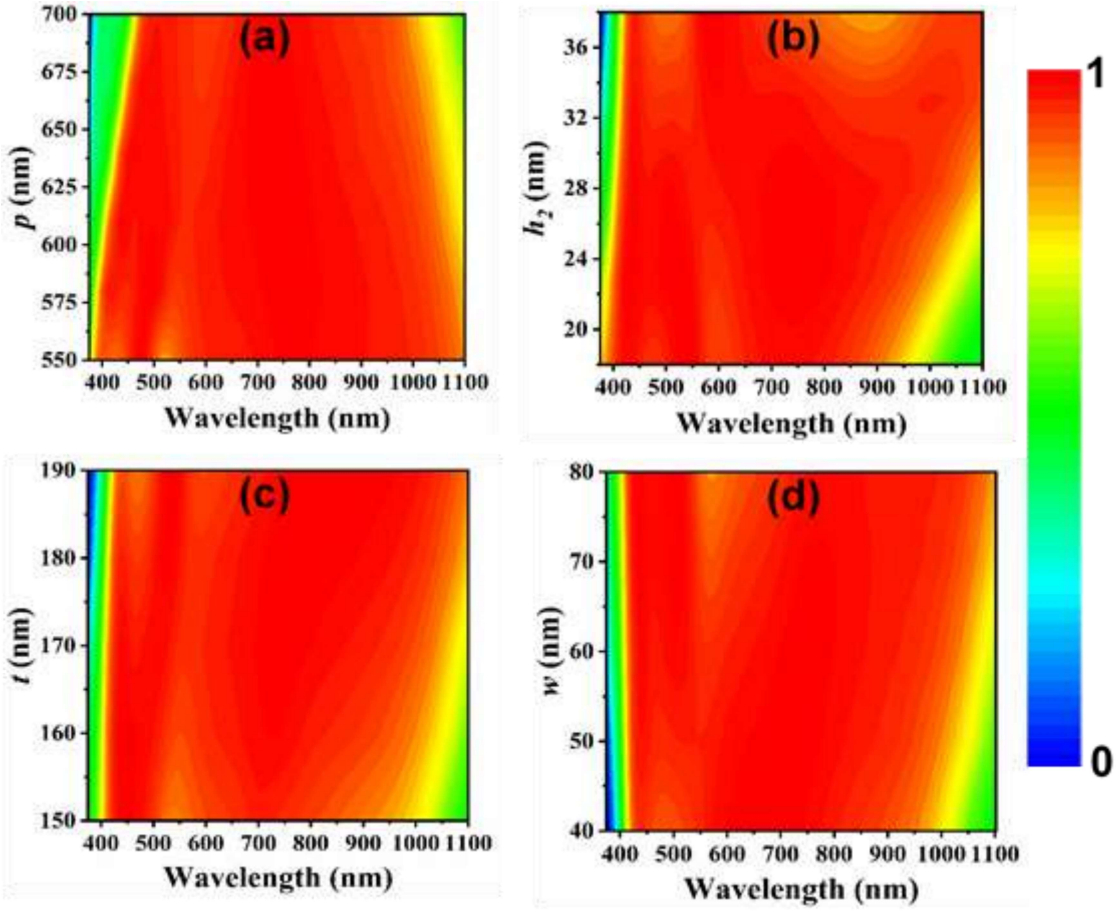

Fig. 4.5 Absorption performances with structural parameters. **(a)** period (p), **(b)** thickness (h_2) of the dielectric, **(c)** thickness (t) of the resonator, **(d)** width (w) of the ring-shaped resonator.

4.3.4 Polarization and incident angle effect

The analysis as mentioned above consigns to the absorbance characteristics of the incident EM waves at a normal angle. As we know that the light source is incident on the device at an oblique angle, and strong absorption with a large angle is valuable for designing the absorber. To obtain the high performance of the absorber, it is necessary to understand the influence of the incident angles for both TE and TM modes. The direction of the solar radiation changes every time, and some parts of the radiation incident on the unit cell in the form of unpolarized radiation. Thus, a convenient metamaterial unit cell design must operate for all the

incident EM radiations for optimizing the absorption coefficient. Therefore, the absorption values of the proposed metamaterial absorber must be independent for both TE and TM polarization radiation because the design is symmetrical, so all the absorption remains the same for all the polarization angles. Thus, the simulated absorption results for both TE and TM waves at different polarisation angles are shown in Fig. 4.6(a) and 4.6(b), where the angles are changed from 0°-80° at 20° intervals. The angle of polarization in the x-y plane for both cases can be defined as the angle variation. From the obtained result, it be can be seen that the polarization angle independent of TE and TM modes within the complete working in broadband. The polarization angle is very important for designing a metamaterial absorber because the required absorption is necessary for solar harvesting energy. Fig. 4.6(c) and 4.6(d) show the contrast of light absorption for the different incident angles. In TE polarization, when the incident angles are more significant than 450, the absorption efficiency is weakened, which shows approximately 90% absorption, because the magnetic field direction varies with the incidence angle, due to which the strength of the magnetic resonant decreases. In the TE polarization case, the absorption bandwidth is above 95% up to 450 in the 420-1100 nm wavelength region, while the 90% absorption maintains the angles 450-600 in that region. The absorption bandwidth is increased with different incident angles compared to the TM polarization because the magnetic field is held when changed the incident angles with resonant peaks. So, it's the best choice for sensing applications under large incidence angles because it maintained broadband absorption in the Visible-NIR region.

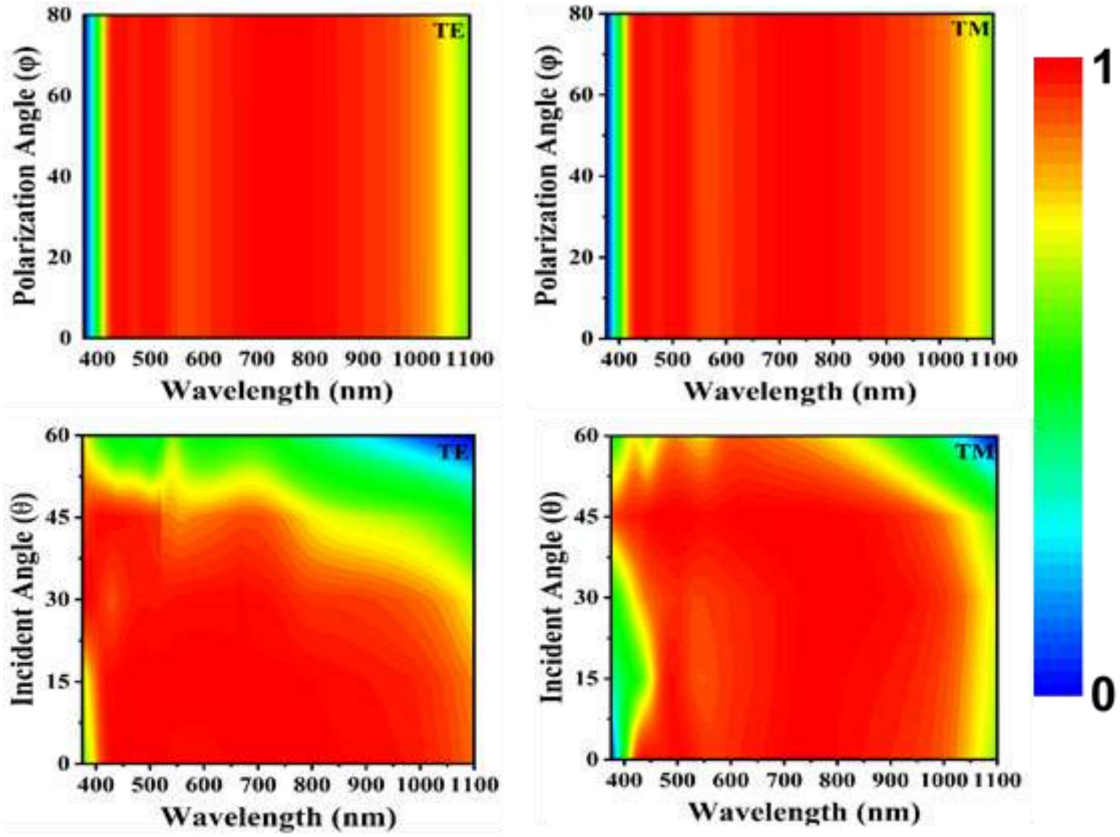

Fig. 4.6 (a, b) Normal and oblique polarization angle from 0°-80°, **(c, d)** normal and oblique incident angle from 0°-60° for TE and TM modes, respectively.

4.3.5 Absorption with different dielectric materials

The bottom plane of the tungsten metal is replaced with other metals (Au, Ag, Al, and Cr), and compared all absorption spectra without changing any thickness and dimensions[128]. The simulated structure of the metamaterial absorber for selective metals reveals more significant results because it shows the coupling of surface Plasmon, which helps achieve perfect absorption. The responses of these absorbers for the Visible-NIR regime are plotted in Fig. 4.7(a). The absorber's optimized absorption with tungsten-based configurations is indicated in the plot, where the absorption of chromium (Cr) is close. Noble metals (Ag, Au, and Al) are not giving much more absorption than tungsten. We observed the ultra-thin

dielectric spacer layer for the proposed absorber. In the proposed absorber, a GaAs semiconductor is used with a high dielectric constant. Therefore, the ultra-thin GaAs layer is expected to be responsible for the absorption in the broadband region. When GaAs are replaced by a different dielectric spacer such as SiO2, SiN. Si, and ITO, observed results are displayed in Fig. 4.7(b), and their comparisons are discussed here. The absorption intensity, high dielectric constant, and larger bandwidth are observed for the GaAs compared to the other dielectric spacer. Silicon (Si) gives a better absorption spectrum that is close to the GaAs. Significantly, the absorption and bandwidth decreased in the structure with decreased dielectric constant due to the limitation of fields and the significantly reduced excitation.

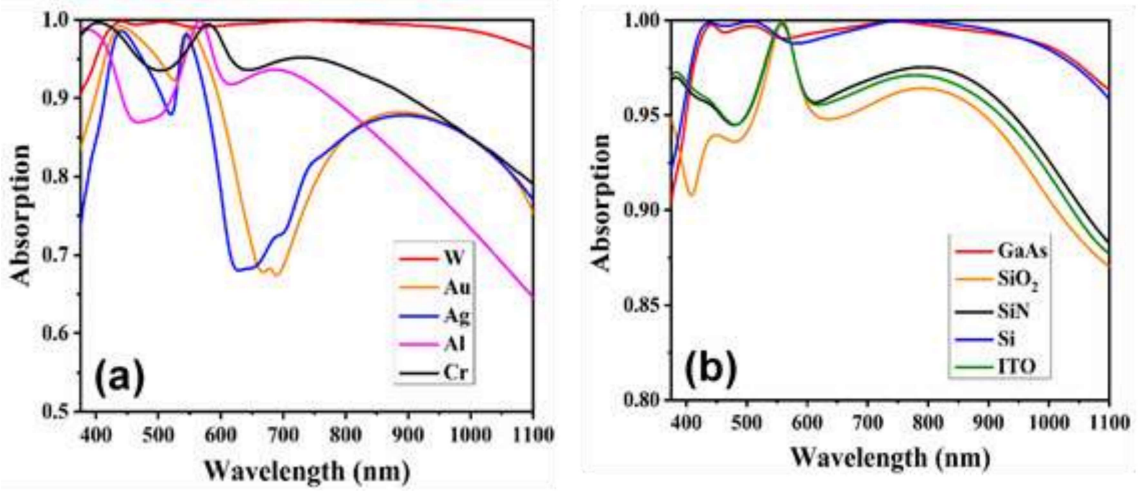

Fig. 4.7 Absorption spectra of the absorber, **(a)** different metals of the bottom layer, **(b)** different dielectric layers.

4.3.6 Comparative study

In Table 4.2, we have discussed the absorption features and displayed their comparisons with previous absorber designs, wavelength range, dimensions, materials, and absorption level. Perfect absorbers (Visible to NIR) are rarely found, operating the entire regions based on three layers. Moreover, we obtain a larger bandwidth than other absorbers

and absorption, which is above 95% in this region. The main reasons for high absorption match the impedance of the bottom layer (tungsten). Nothing that the multiple-layers structures increase the sample size but also increase the cost, which is not conducive to its integrated development. In our proposed absorber, we have used a square ring-shaped, which improves absorptivity compared to other structures. The active regions, number of layers, dimensions, absorption level, and peak absorption for different dielectric materials are tabulated in Table 4.2.

Table 4.1 Comparison of the designed metamaterial absorber with previously reported research papers.

Refs.	Range (nm)	Total layers	Dimensions (w*l*h) in nm	Materials	Absorption level	Peak absorption
166	262-709	Two	240*240*170	Au, Si	Above 90%	99.1%
195	389.34-697.19	Three	1000*1000*225	W, SiO_2	Above 91.24%	99.99
196	430-1400	Three	690.5*90.5*410	Al, GaAs	Not a broadband absorber	Three peaks (99.99%)
197	437.9-578.3	Three	300*300*272	Au, SiO_2, Si	Above 80%	98.2%
169	430-850	Three	320*320*50	Au, SiO_2	Above 90%	99%
170	400-850	Three	500*500*174	Al, SiO_2	Not a broadband absorber	Two peaks (92% & 99.99%)
This work	375-1100	Three	610*610*398	W, GaAs	Above 90%	99.94%

4.3.7 Constitutive electromagnetic parameters retrieval

The constitutive EM parameters viz., magnetic susceptibility (χ_{ms}), and electric susceptibility (χ_{es}) can be evaluated from Eqs. 4.8 and 4.9 with a co-polarized reflection coefficient[198]. Here, d is the thickness of the spacer layer, and k_o is the wavenumber. This method is used for the extraction of constitutive parameters, which do not involve the S_{21}

parameters. The extracted parts (imaginary and real) of effective permittivity (ε_{eff}) and effective permeability (μ_{eff}) are can be calculated by Eqs. 4.10 and 4.11 which are demonstrated in Fig.4.8(a) and 4.8(b), respectively[142]:

$$\chi_{es} = \frac{2j}{k_0}\frac{1 - S_{11}}{1 + S_{11}} \tag{4.8}$$

$$\chi_{ms} = \frac{2j}{k_0}\frac{1 + S_{11}}{1 - S_{11}} \tag{4.9}$$

$$\varepsilon_{eff} = 1 + \frac{\chi_{es}}{d} \tag{4.10}$$

$$\mu_{eff} = 1 + \frac{\chi_{ms}}{d} \tag{4.11}$$

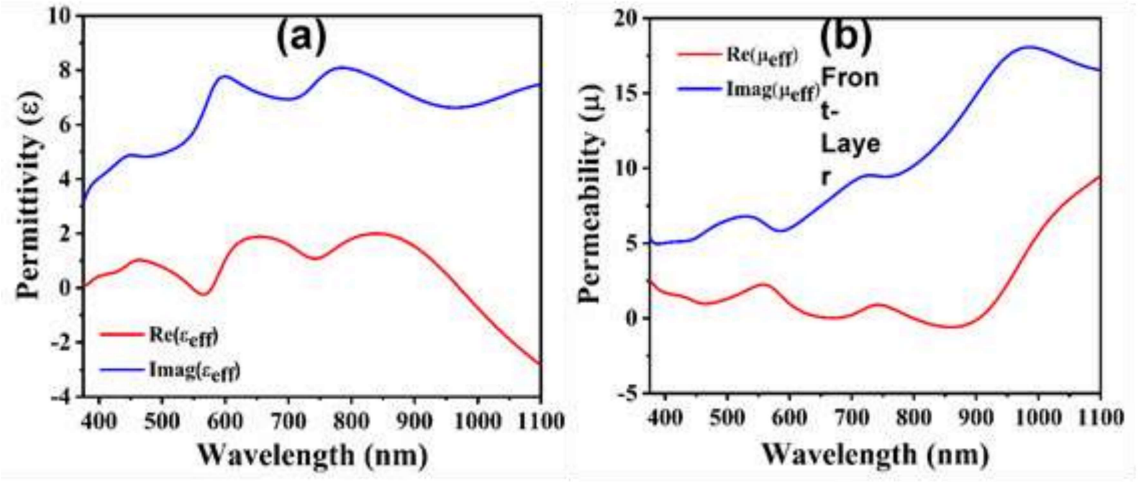

Fig. 4.8 Extracted constitutive electromagnetic parameters of the absorber, **(a)** real and imaginary permittivity, **(b)** real and imaginary permeability.

4.3.8 Performance evaluation of conversion efficiency

Various structure of absorber shows the different absorption under the solar spectrum ($A_{AM1.5}$) of the solar cell. The high conversion efficiency represents the large value of $A_{AM1.5}$ as shown in Fig. 4.9. The proposed absorber provides the broadband absorbance in the spectrum from the visible to near-IR region. We used this expression to obtain the $A_{AM1.5}$ of a solar cell[143],

$$A_{AM1.5} = \frac{\int_{375nm}^{1100nm} A\,(\lambda)\, G(\lambda)\, d\lambda}{\int_{375nm}^{1100nm} G(\lambda)\, d\lambda} \tag{4.12}$$

Where A(λ) and G(λ) represent the absorption of absorber and photon numbers of distribution as a function of wavelength in the solar irradiance (AM1.5) is given as $G(\lambda) = \frac{w(\lambda)}{E(\lambda)}$, where E(λ) and w(λ) is photon energy and solar irradiance. Table 4.3, represent the evaluated values of $A_{AM1.5}$ with the various thickness (h_2) of a dielectric layer of GaAs corresponding to Fig. 4.9. We achieved the larger value of $A_{AM1.5}$ ~99.11% for h_2 = 28 nm, which indicates the high conversion efficiency of a solar cell.

Table 4.2 $A_{AM1.5}$ with different thicknesses (h_2) of GaAs layer.

Thickness (h_2)	**13 nm**	**18 nm**	**23 nm**	**28 nm**	**33 nm**	**42 nm**
$A_{AM1.5}$ (%)	96.84 %	98.07%	98.88%	99.11%	98.74%	97.80%

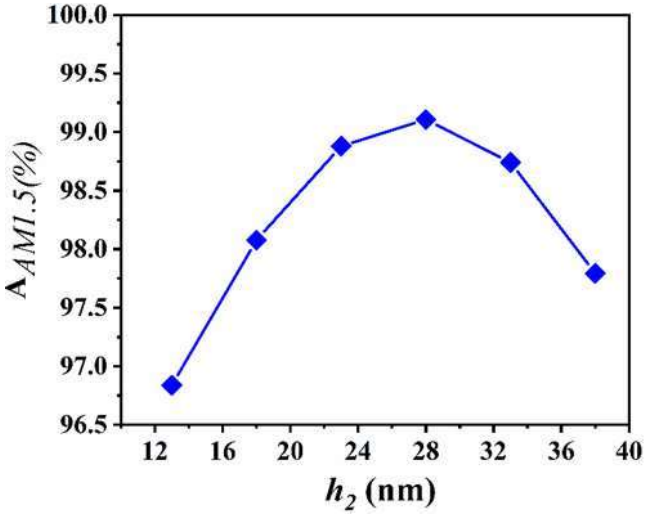

Fig. 4.9 The conversion efficiency ($A_{AM1.5}$) with the various thickness (h_2) of the dielectric layer

4.3.9 Performance evaluation of short circuit current density and solar spectrum

The short-circuit current density (J_{sc}) is also playing a crucial role along with conversion efficiency for solar cells. Fig. 4.10(a) shows a J_{sc} with different thicknesses of the GaAs layer. The electron-hole pairs generated by each absorbed photon, so J_{sc} can be calculated by this expression under the solar illumination[137],

$$J_{sc} = \frac{e}{hc}\int_{375nm}^{1100nm} \lambda\, \Phi_{AM1.5}(\lambda)\, A(\lambda)\, d\lambda \tag{4.13}$$

Where, e, h, c, and λ are electron charge, Plank constant, speed of light, and operating wavelength, respectively. A(λ) and $\Phi_{AM1.5}(\lambda)$ are absorptions of the absorber and solar irradiance. Here, we consider the 100% internal quantum efficiency. When the thickness (h_2) of the GaAs layer is tuned from 13 nm to 38 nm with an interval of 5 nm, J_{sc} is continuously affected by different thicknesses because J_{sc} strongly depends on the resonant modes number in operating wavelength. Table 4.4, represents the different values of J_{sc} with the thickness (h_2). For h_2 = 28 nm, J_{sc} achieved a high value (41.28 mA/cm^2) that is much larger than the reported work[137,147,199].

Table 4.3 J_{sc} with different thicknesses (h_2) of GaAs layer

Thickness (h_2)	**13 nm**	**18 nm**	**23 nm**	**28 nm**	**33 nm**	**42 nm**
J_{sc}(mA/cm^2)	40.34	40.85	41.18	41.28	41.13	40.73

The response of absorber absorption is usually used to calculate the collection of solar energy. The wide bandwidth of wavelength and near-unity absorbance mainly present the ideal absorber. We investigated the illumination of the solar absorption of the absorber under the AM1.5 source in Fig. 4.10(b). The absorbed solar energy and the missed solar energy of the

presented absorber are also calculated shown as in Fig. 4.10(c). This absorber has perfect absorption so the light capture efficiency is very high. Therefore it shows very low missed solar energy. The multiple resonance coupling is responsible to achieve the perfect absorption in the broadband wavelength range[200]. Therefore, the strong resonance absorption of solar cells can be used the solar harvesting, solar cell, and thermal emission-related potential applications.

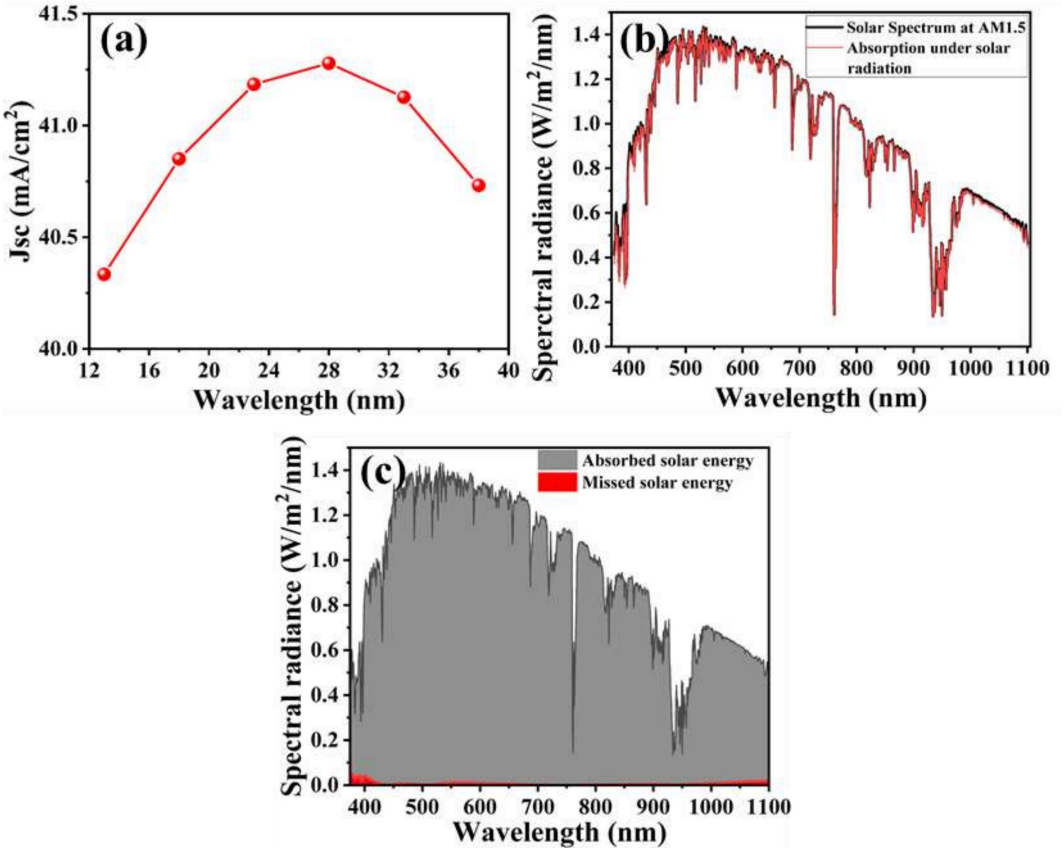

Fig. 4.10 (a) Calculated short circuit current density (J_{sc}) with different thicknesses (h_2) of GaAs layer, **(b)** absorbed energy of proposed absorber in AM1.5 solar spectrum, **(c)** absorbed solar energy and missed solar energy in the applied range of solar radiance.

4.4 Conclusions

In this chapter, the broadband and highly efficient tungsten-based nano-absorber has been investigated. The proposed absorber has higher stability with a square ring-shaped nanostructure in terms of higher melting temperature, spectrum, and efficiency. The

symmetrical geometry of the top layer makes it polarization insensitive. Significant impedance matching achieves effective absorption for this design which can also exhort the resonance front-layer and intrinsic loss in the back-layer. The proposed perfect metamaterial absorber demonstrates nearly perfect absorption of over 98% in the broadband region (375-1100nm). We have observed high absorption bands at the wavelengths 441.80 nm, 506.88 nm, and 744.01 nm, where absorption is greater than 99%. The absorption band's position and amplitude can be tuned with resonators' parameters and the constituted dielectric layer's thickness. We have also studied the effects of polarization angles and incident angles for both TM and TE modes. The proposed absorber holds the solar cell application because the improved conversion efficiency ($A_{AM1.5}$) is very large. Moreover, it has a large short circuit current density (41.28 mA/cm^2) and also obtained the near-unity solar due to multiple coupling of resonances in the broadband range. Therefore proposed absorber opens a new door in the visible to near-infrared wavelength region paradigm to design multiple potential applications.